ELSEVIER

Comput. Methods Appl. Mech. Engrg. 190 (2001) 4569–4585

Computer methods in applied mechanics and engineering

www.elsevier.com/locate/cma

Fourier series method for plane elastic problems of polygonal domain

Jiann-Gang Deng, Fu-Ping Cheng *

Department of Civil Engineering, National Chiao Tung University, 1001 Ta Hsueh Road, Hsinchu, Taiwan, ROC

Received 1 February 1999; received in revised form 18 April 2000

Abstract

This study employs the Fourier series method based on the edge function approach to solve the plane elastic problem of polygonal domain described by Navier equations. The analytical solutions serve as a set of fundamental solutions for each edge. Superposing the solution function and matching the prescribed boundary conditions in each edge allows the solving of the unknown variables and the analysis of the problem. An extra corner function and regularization technique is utilized to enhance convergence rate. Only one element is required to analyze which polygon domain is convex, however, by dividing a non-convex shape into several convex shapes, the proposed method can be extended to irregular geometrical shape. Numerical examples demonstrate the merits of the developed scheme, as well as its efficiency and accuracy.

1. Introduction

Linear elastic isotropic behavior is commonly assumed for stress analysis of solids in civil and mechanical engineering. Additionally, most solution schemes were developed for plane elastic problems and later extended to other fields of engineering. However, realistic engineering problems are solved only through numerical methods with the most popular methods being FDM, FEM and BEM. Although these methods have been very successful, their common drawback is their inefficiency in computation or problem modeling. These findings provide motivation for developing an efficient numerical method.

The Fourier series method based on the edge functions has already been successfully applied to solve various boundary value problems. Bird and Steele [1,2] applied this method to analyze the bending problem of circular plate. Kwok surveyed the mode III fracture mechanics analysis [3], and later extended the problem to cracks in the polygonal shell of revolution [4]. Furthermore, Kang [5] developed a procedure to analyze the polygonal plate-bending problem. Also, Wu [6,7] applied the method in question to the stability of shallow shell. Fu and Steele [8] applied it to the Dugdale crack in a cylindrical shell, and Fu [9] extended this method to the in-plane and bending problems of the shallow shell. Gorman [10] presents vibration analysis of plates by this approach. However, most of these researches were aimed to second- and fourth-order differential equations governed by the Laplace's equation. This study employs the Fourier series method to solve a boundary value problem described by two coupled second-order partial differential operators, the Navier equations governing the plane elastic problem of the polygonal domain. The basic steps in the method are as follows:

* Corresponding author.

0045-7825/01/$ - see front matter
PII: S0045-7825(00)00333-9

1. Find the fundamental solutions that satisfy the plane elastic governing equation. By solving a half-plane elastic problem with periodic boundary inputs, the fundamental solutions based on the Fourier series expansion are derived. These solutions will serve as the edge function for each side of the polygonal.
2. Calculate the interaction coefficients in each edge. The solution functions derived in step 1 can be used to calculate the Fourier harmonic coefficients for all edges in response to the contribution from each of these edge functions.
3. Superposing the contributions from all edges and matching the prescribed boundary conditions. The summation of the edge functions described by Fourier harmonic involved unknown coefficients, which must be matched to the prescribed boundary condition. Therefore, a system of equations is constructed by assembling the interaction coefficients and the unknown variables in a matrix form.

Although the exponential decaying term of analytical solutions served as a solution function, leading to the matrix being diagonally dominant, the present method is restricted to the domain must be convex. However, by partitioning the domain into several convex sub-domains, an effective scheme proposes element connection by satisfying appropriate continuity conditions accounting for why this method can be extended to the irregular domain. The main drawback of the proposed method is its low convergence rate due to the Gibb's phenomenon. Two regularization techniques including arithmetic mean sequences and general character σ factor are employed to improve the convergence rate [11,12]. Furthermore, an extra corner function is used to promote the convergence rate in the corner boundary condition. Thus, the proposed method can be utilized more efficiently.

Similar to the boundary integral method, this approach requires no mesh generation, and the number of elements and degrees of freedom are significantly smaller than the FEM, FDM. The advantage of this approach over boundary elements is that the matrices are well-conditioned. By combining plate-bending problems, this approach can be extended to the plated structures.

2. Governing equation and solution function

The governing equations of isotropic elastic continuum for plane elasticity with elastic support are illustrated as follows, where gravitation is absent [13]:

$$\frac{\partial \sigma_x}{\partial x} + \frac{\partial \tau_{xy}}{\partial y} - k_d^2 u = 0, \tag{1a}$$

$$\frac{\partial \tau_{yx}}{\partial x} + \frac{\partial \sigma_y}{\partial y} - k_d^2 v = 0 \quad \text{in } \Omega, \tag{1b}$$

$$u_N^* = d_1(s), \quad v_N^* = d_2(s) \quad \text{on } \partial\Omega_1, \tag{1c}$$

$$\sigma_N^* = d_3(s), \quad \tau_N^* = d_4(s) \quad \text{on } \partial\Omega_2, \tag{1d}$$

where, $k_d^2 = k_s/E(1-v^2)$, k_s denotes the spring constant of the elastic support. Regarding numerically treating difficulty to the constant term of the solution of Eqs. (1a)–(1d) k_s is introduced. An extremely small k_s will not induce an accuracy problem in the absence of elastic support. According to Fig. 1, Ω represents a polygonal domain, and u, v, σ, τ, denote the displacements and stresses in Ω. The relations of displacements u, v and stresses σ, τ in terms of axes x, y are defined as:

$$\sigma_x = \frac{E}{1-v^2}(u_x + v \times v_y), \tag{2a}$$

$$\sigma_y = \frac{E}{1-v^2}(v_y + v \times u_x), \tag{2b}$$

$$\tau_{xy} = \frac{E}{2(1+v)}(u_y + v_x), \tag{2c}$$

where u_x, u_y, v_x, v_y are derivatives of displacements u, v, and E, v denote the elastic modulus and Poisson's ratio, respectively.

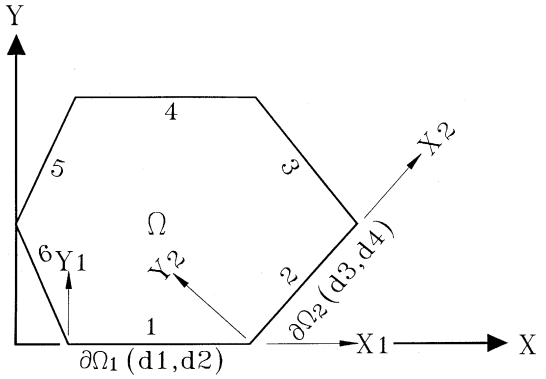

Fig. 1. Edge coordinate system of analysis plane.

Four kinds of possibly prescribed boundary values in the outward normal direction to the edge include displacements u_N^*, v_N^* and stresses σ_N^*, τ_N^*. Two of these four quantities are ranked to construct appropriate boundary conditions. The four types of boundary condition used are

$$BC_1 = \begin{Bmatrix} u_N^* \\ v_N^* \end{Bmatrix}, \quad BC_2 = \begin{Bmatrix} \sigma_N^* \\ \tau_N^* \end{Bmatrix}, \quad BC_3 = \begin{Bmatrix} v_N^* \\ \tau_N^* \end{Bmatrix}, \quad BC_4 = \begin{Bmatrix} \sigma_N^* \\ u_N^* \end{Bmatrix}.$$

By applying the method of separation variables, the general solution of Eqs. (1a)–(1d) can be derived as follows, herein, the exponential decay part of the solution is used for the half-plane problem.

$$u = \sum_{n=1}^{\infty} a_n e^{-p_n y} \sin(\lambda_n x) + b_n e^{-q_n y} \sin(\lambda_n x), \tag{3a}$$

$$v = a_0 e^{-q_0 x} + b_0 e^{-p_0 y} + \sum_{n=1}^{\infty} a_n c_n e^{-p_n y} \cos(\lambda_n x) + b_n d_n e^{-q_n y} \cos(\lambda_n x), \tag{3b}$$

where

$$p_0 = k_d, \quad q_0 = k_d\sqrt{2/(1-\nu)}, \quad p_n = \sqrt{\lambda_n^2 + k_d^2}, \quad q_n = \sqrt{\lambda_n^2 + k_d^2 2/(1-\nu)},$$
$$c_n = p_n/\lambda_n, \quad d_n = q_n/\lambda_n, \lambda_n = n\pi/l_i.$$

l_i represents the length of edge i, which the boundary inputs represented by Fourier cosine expansions along $y_i = 0$ as in Fig. 2. λ_n represents the mode number of l_i, and unknown coefficients a_n, b_n are the amplitude of mode n.

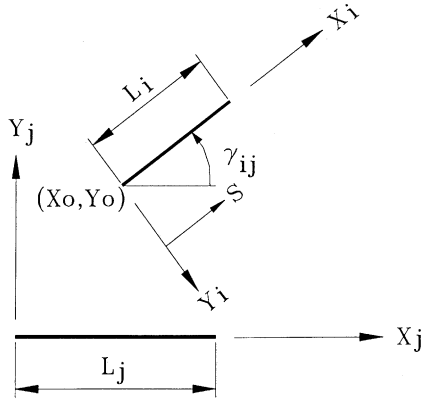

Fig. 2. Coordinate transform on edge i and j.

3. Construct Fourier series coefficient matrix

According to Fig. 1, each edge has defined a local coordinate system that represents a half-plane problem. Additionally, the displacement and stress on each edge must satisfy the solutions of governing equations. Therefore, the problem can be calculated by superposition of the edge solutions from all the half-plane problems. However, the boundary values on each edge are contributed by each local solution, and hence, the influence coefficients on each edge can be calculated from all local coordinate. As an example of edge i, j (Fig. 2), where displacements u_j, v_j exist on edge j, the influence of displacements and stresses on edge i can be calculated from the coordinate transformation as

$$u_j^i = u_j \cos\gamma_{ij} + v_j \sin\gamma_{ij}, \tag{4a}$$

$$v_j^i = u_j \sin\gamma_{ij} - v_j \sin\gamma_{ij}, \tag{4b}$$

$$(\sigma_N)_j^i = \frac{E}{1-v^2}\{(u_j)_x(\sin^2\gamma_{ij} + v\times\cos^2\gamma_{ij}) + (v_j)_y(\cos^2\gamma_{ij} + v\times\sin^2\gamma_{ij}), - (1-v)((u_j)_y + (v_j)_x)\sin\gamma_{ij}\cos\gamma_{ij}\}, \tag{4c}$$

$$(\tau_N)_j^i = \frac{E}{2(1+v)}\{(v_j)_x(\sin^2\gamma_{ij} - \cos^2\gamma_{ij}) + (u_j)_y(\sin^2\gamma_{ij} - \cos^2\gamma_{ij}), + ((u_j)_x - (v_j)_y)\sin 2\gamma_{ij}\}, \tag{4d}$$

where γ_{ij} represents an angle between edge j and i, $(u_j)_x, (u_j)_y, (v_j)_x, (v_j)_y$, are derivatives of u_j, v_j. The series terms in Eqs. (3a) and (3b), $e^{-p_n y}\cos(\lambda_n x), e^{-p_n y}\sin(\lambda_n x), e^{-q_n y}\cos(\lambda_n x), e^{-q_n y}\sin(\lambda_n x)$ are introduced by the following expansions:

$$e^{-p_n y}\cos(\lambda_n x) = \sum_{m=0}^{\infty}(C_{mn}^{p_n})_j^i \cos(\alpha_m s), \tag{5a}$$

$$e^{-p_n y}\sin(\lambda_n x) = \sum_{m=0}^{\infty}(D_{mn}^{p_n})_j^i \cos(\alpha_m s), \tag{5b}$$

$$e^{-q_n y}\cos(\lambda_n x) = \sum_{m=0}^{\infty}(C_{mn}^{q_n})_j^i \cos(\alpha_m s), \tag{5c}$$

$$e^{-q_n y}\sin(\lambda_n x) = \sum_{m=0}^{\infty}(D_{mn}^{q_n})_j^i \cos(\alpha_m s), \tag{5d}$$

where $(C_{mn}^{p_n})_j^i, (D_{mn}^{p_n})_j^i, (C_{mn}^{q_n})_j^i, (D_{mn}^{q_n})_j^i$ are derived in Appendix A.

Concerning an arbitrary boundary value $d_j(x)$ existing on edge j, this value can be replaced by the Fourier cosine expansion along axis x_j .

$$d_j(x) = \sum_{m=0}^{\infty}(d_m)_j \cos(\alpha_m x_j), \tag{6}$$

where $(d_m)_j$ represents the mth coefficient of the function of $d_j(x)$. Herein, the periodically extended function is served as the boundary condition of a half-plane problem. Combining Eqs.(3a) and (3b), Eqs. (4a)–(4d), (5a)–(5d), the displacements and stresses of the mth term of influence functions from edge j to edge i are expressed by Fourier series as follows, where the nhj harmonic terms are employed to analyze the problem.

$$((u_N)_m)_j^i = \sum_{n=0}^{nhj-1} ((u1_{mn})_j^i \times a_n^i + (u2_{mn})_j^j \times b_n^i), \tag{7a}$$

$$((v_N)_m)_j^i = \sum_{n=0}^{nhj-1} ((v1_{mn})_j^i \times a_n^i + (v2_{mn})_j^i \times b_n^i), \tag{7b}$$

$$((\sigma_N)_m)_j^i = \sum_{n=0}^{nhj-1} ((s1_{mn})_j^i \times a_n^i + (s2_{mn})_j^i \times b_n^i), \tag{7c}$$

$$((\tau_N)_m)_j^i = \sum_{n=0}^{nhj-1} ((t1_{mn})_j^i \times a_n^i + (t2_{mn})_j^i \times b_n^i). \tag{7d}$$

Definitions of $(u1_{mn})_j^i, (u2_{mn})_j^i, (v1_{mn})_j^i, (v2_{mn})_j^i, (s1_{mn})_j^i, (s2_{mn})_j^i, (t1_{mn})_j^i, (t2_{mn})_j^i$, are derived in Appendix B.

For each edge, the coefficients of any Fourier series term accumulated from all edges must have the same value as the prescribed boundaries. From Eqs. (6) and Eqs. (7a)–(7d), by simply equating the boundary values, the system of simultaneous equation can be constructed as

$$\begin{bmatrix} (DM_{mn})_1^1 & (DM_{mn})_2^1 & \cdots & \cdots & (DM_{mn})_M^1 \\ (DM_{mn})_1^2 & (DM_{mn})_2^2 & \cdots & \cdots & (DM_{mn})_M^2 \\ (DM_{mn})_1^3 & (DM_{mn})_2^3 & \cdots & \cdots & (DM_{mn})_M^3 \\ \vdots & \vdots & \ddots & (DM_{mn})_j^i & \vdots \\ (DM_{mn})_1^N & (DM_{mn})_2^N & \cdots & \cdots & (DM_{mn})_M^N \end{bmatrix} \begin{bmatrix} (C_n)^1 \\ (C_n)^2 \\ (C_n)^3 \\ \vdots \\ (C_n)^N \end{bmatrix} = \begin{bmatrix} (d_m)_1 \\ (d_m)_2 \\ (d_m)_3 \\ \vdots \\ (d_m)_M \end{bmatrix}, \tag{8}$$

where $(C_n)^i = \{ a_n^i \quad b_n^i \}^{\mathrm{T}}$, is the unknown coefficient of edge i, and $(d_m)_j$ denotes the prescribed boundary value on edge j. Regarding Dirichlet problems, boundary condition is

$$\{d_m\}_j = \{ ((u_N)_m)_j \quad ((v_N)_m)_j \}^{\mathrm{T}} \tag{9a}$$

and the corresponding influence coefficients matrix is:

$$(DM_{mn})_j^i = \begin{bmatrix} (u1_{mn})_j^i & (u2_{mn})_j^i \\ (v1_{mn})_j^i & (v2_{mn})_j^i \end{bmatrix} \tag{9b}$$

for Neumann problems, boundary condition is:

$$\{d_m\}_j = \{ ((\sigma_N)_m)_j \quad ((\tau_N)_m)_j \}^{\mathrm{T}} \tag{9c}$$

and the corresponding influence coefficients matrix is:

$$(DM_{mn})_j^i = \begin{bmatrix} (s1_{mn})_j^i & (s2_{mn})_j^i \\ (t1_{mn})_j^i & (t2_{mn})_j^i \end{bmatrix} \tag{9d}$$

For the mixed boundary conditions, substituting an exact u, v, s, t to calculate the coefficients of sub-matrix $(DM_{mn})_j^i$ is convenient.

A system of simultaneous equations has been developed from Eqs. (9a)–(9d) and can easily be solved by any linear equation solver. The displacements and stresses at any point of domain can be calculated under global coordinates, defined as

$$u = \sum_{j=1}^{N} u_j \cos\gamma_j - v_j \sin\gamma_j, \tag{10a}$$

$$v = \sum_{j=1}^{N} u_j \sin\gamma_j + v_j \cos\gamma_j, \tag{10b}$$

$$\sigma_x = \frac{E}{1-v^2} \sum_{j=1}^{N} \Big[(u_j)_x (\cos^2\gamma_j + v \times \sin^2\gamma_j) + (v_j)_y (\sin^2\gamma_j + v \times \cos^2\gamma_j) - (1-v)((v_j)_x + (u_j)_y) \sin\gamma_j \cos\gamma_j \Big], \tag{10c}$$

$$\sigma_y = \frac{E}{1-v^2} \sum_{j=1}^{N} \Big[(u_j)_x (\sin^2\gamma_j + v \times \cos^2\gamma_j) + (v_j)_y (\cos^2\gamma_j + v \times \sin^2\gamma_j) + (1-v)((v_j)_x + (u_j)_y) \sin\gamma_j \cos\gamma_j \Big], \tag{10d}$$

$$\tau_{xy} = \frac{E}{2(1+v)} \sum_{j=1}^{N} \Big[(u_j)_y (\cos^2\gamma_j - \sin^2\gamma_j) + (v_j)_x (\cos^2\gamma_j - \sin^2\gamma_j) + ((u_j)_x - (v_j)_y) \sin 2\gamma_j \Big]. \tag{10e}$$

u_j, v_j is defined as Eqs. (4a)–(4d), which represents the displacement of point j, but coordinates x, y in Eqs. (4a)–(4d) should be replaced by x_j, y_j, where x_j, y_j, represent the relative coordinate of the unknown point on the jth local coordinate system. Meanwhile, γ_j indicates the angle between the global coordinate system and jth local coordinate system, and N denotes the total number of defined edges.

To verify the feasibility of the proposed method, an example with a simple geometry was tested (Fig. 3), comprising a symmetrical plane with two opposite free edges, fixed in the bottom face, and supporting a 1000 uniform distributed load on the top. Four boundary conditions are assigned as $d = [BC_1^1 \quad BC_2^2 \quad BC_2^3 \quad BC_2^4]^{\mathrm{T}}$. The prescribed values in each of the edges are zero except for $\{BC_2^3\} = [1000 \quad 0 \quad \cdots]^{\mathrm{T}}$. This example was analyzed by the approach with 33 harmonics and ANSYS [14] with 400 elements. The two results are then compared. According to Fig. 4, the deformed shape is attributed to the 33 harmonics that are given. Compared with ANSYS along edge $\bar{A}\bar{D}$, $\bar{C}\bar{D}$, and the interior of plane $\bar{E}\bar{F}$, $\bar{G}\bar{H}$, (Figs. 5–8), the solutions of these locations are very close for both displacement and stress. In some distance from boundary, both methods yield more accurate results (Figs. 7 and 8). To compare the matrix sizes, 33 harmonics required 272 degrees of freedom, while ANSYS with 400 elements required 882 degrees of

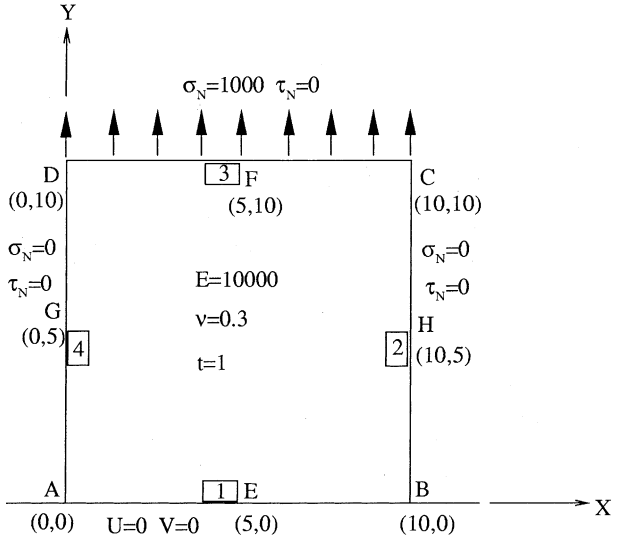

Fig. 3. Plane under uniform axial stress.

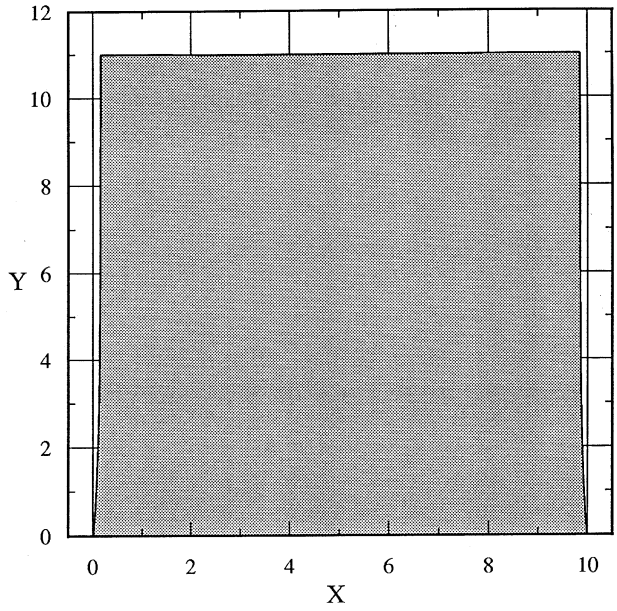

Fig. 4. Plot of deformed shape.

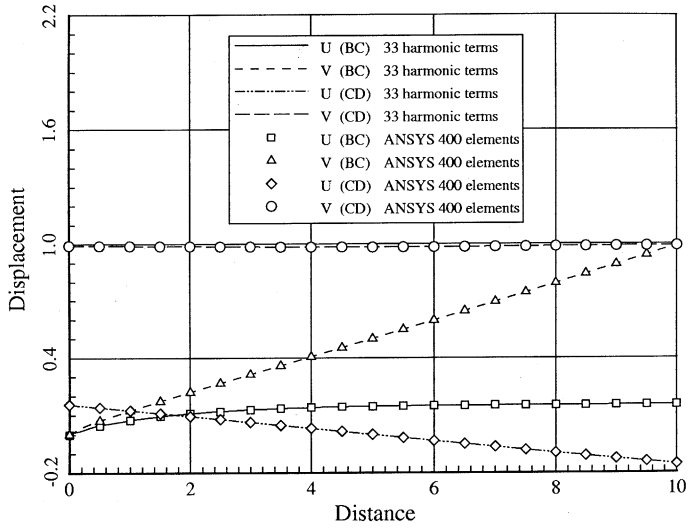

Fig. 5. Comparison of displacements along edge *BC*, *CD*.

freedom, therefore, considerable memory space and CPU time are saved. However, the stress on the corner of fixed edge $\bar{A}\bar{B}$ in this approach differs markedly from the ANSYS results. Additionally, the stresses along the fixed edge oscillate with evident amplitude (Fig. 6). Owing to the non-compatibility of the boundary condition, the Gibb's phenomenon arises in response to the stress discontinuity at the corner of the fixed edge. Consequently, the low convergence rate of stress will reduce the accuracy and efficiency of the proposed method even the more harmonic terms are used. However, the Gibb's phenomenon can be eliminated by regularization techniques. This work introduces the Cesàro procedure and the general character of σ factor to smooth the stress oscillation caused by the Gibb's phenomenon. Comparing Figs. 6, 9 and 10, the stress distribution attribute to 33 harmonics by the Cesàro procedure and the σ factor has demonstrated that the stress oscillation has been eliminated and the results match the ANSYS solution except near corner A, B.

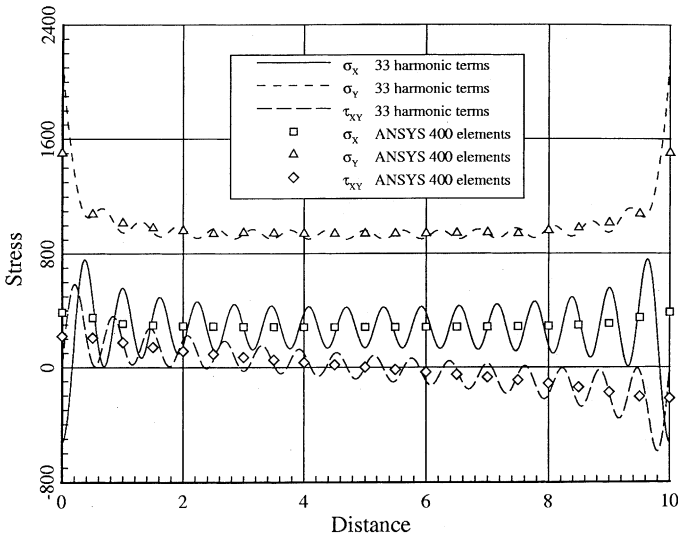

Fig. 6. Comparison of stress along *AB*.

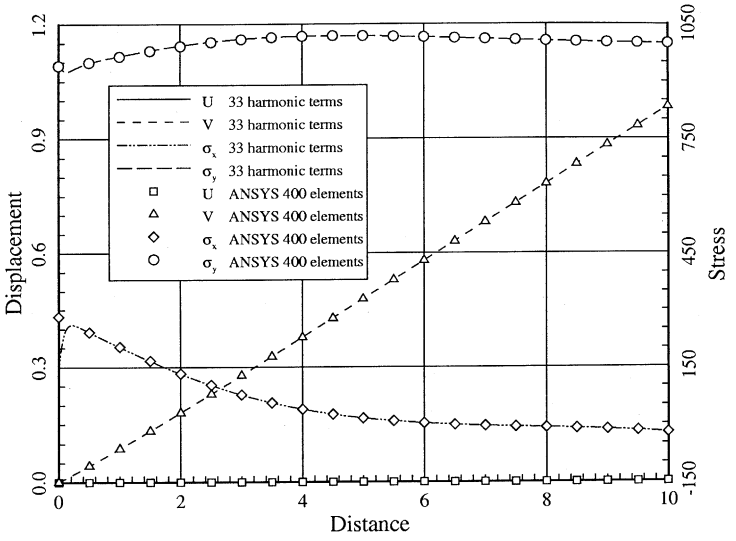

Fig. 7. Comparison of displacements and stresses along edge *EF*.

4. Incorporating corner degree of freedom

Although the Gibb's phenomenon can be eliminated by the regularization technique, the corner stress will lose it accuracy while reducing the amplitude of high frequency terms. However, this shortcomings can be remedied by incorporating the corner singular term. Based on the analytical solution, an extra corner function is defined below:

$$(C_c^{p_c})_j^i = c_c \mathrm{e}^{-p_c y_j^i} \cos(\lambda_c x_j^i), \tag{11a}$$

$$(D_c^{p_c})_j^i = \mathrm{e}^{-p_c y_j^i} \sin(\lambda_c x_j^i), \tag{11b}$$

$$(C_n^{p_n})_j^i = c_n \mathrm{e}^{-p_n y_j^i} \cos(\lambda_n x_j^i), \tag{11c}$$

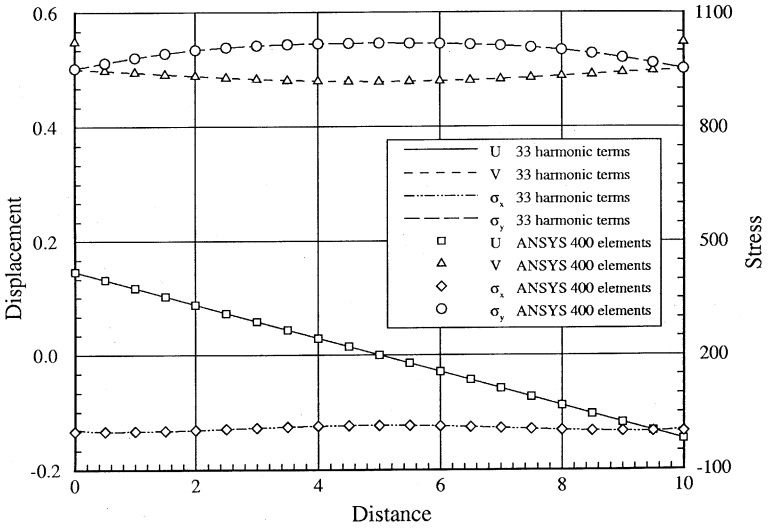

Fig. 8. Comparison of displacements and stresses along GH.

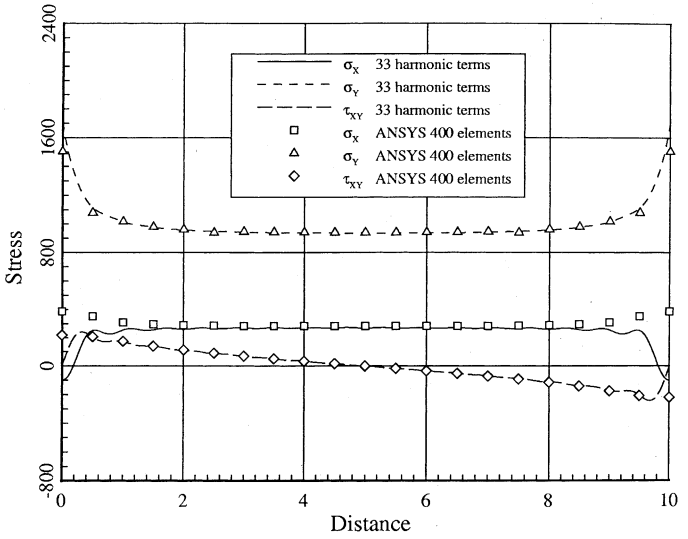

Fig. 9. Comparison of stress along AB smooth by Lanczos method.

$$(D_n^{p_n})_j^i = \mathrm{e}^{-p_n y_j^i}\sin(\lambda_n x_j^i), \tag{11d}$$

$$(C_n^{q_n})_j^i = c_n \mathrm{e}^{-q_n y_j^i}\cos(\lambda_n x_j^i), \tag{11e}$$

$$(D_n^{q_n})_j^i = \mathrm{e}^{-q_n y_j^i}\sin(\lambda_n x_j^i), \tag{11f}$$

where $\lambda_c = \pi/2l_j, (C_c^{p_c})_j^i, (D_c^{p_c})_j^i$ represents the influence coefficients of corner j to corner i, $(C_n^{p_n})_j^i, (D_n^{p_n})_j^i, (C_n^{q_n})_j^i, (D_n^{q_n})_j^i$ the influence coefficients of corner j to edge i, and x_j^i, y_j^i are the relative coordinates of the starting point of edge i on the jth local coordinate system. From Eqs. (11a)–(11f), the displacement of corner i can be defined as:

$$u_c^i = \sum_{j=1}^{N}\left[(D_c^{p_c})_j^i \times a_c^j + \sum_{n=0}^{nhj-1}((D_n^{p_n})_j^i \times a_n^j + (D_n^{q_n})_j^i \times b_n^j)\right], \tag{12a}$$

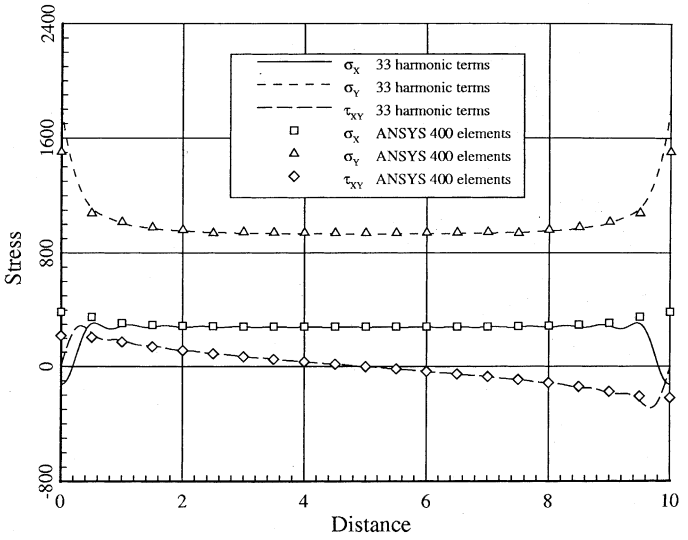

Fig. 10. Comparison of stress along *AB* by Lanczos method.

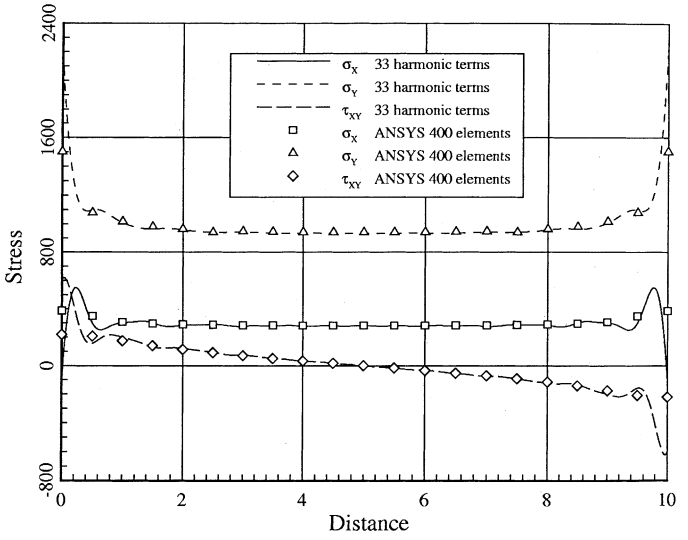

Fig. 11. Comparison of stress along *AB* by incorporating corner function.

$$v_c^i = \sum_{j=1}^{N} \left[(C_c^{p_c})_j^i \times a_c^j + \sum_{n=0}^{nhj-1} ((C_n^{p_n})_j^i \times a_n^j + (C_n^{q_n})_j^i \times b_n^j) \right]. \tag{12b}$$

Herein, coordinate transformation was used by substituting u_c^i, v_c^i and their derivatives into Eqs. (4a)–(4d). Therefore, the influence coefficients of displacement and stress at corner i can be calculated from corner j and edge j.

By rearranging Eqs. (9a)–(9d), for the Dirichlet problems, $(DM_{mn})_j^i$ and $\{d_m\}_j$ is modified as

$$(DM_{mn})_j^i = \begin{bmatrix} (u1_{mn})_j^i & (u2_{mn})_j^i & ((a21)_m)_j^i \\ (v1_{mn})_j^i & (v2_{mn})_j^i & ((a31)_m)_j^i \\ ((a12)_n)_j^i & ((a13)_n)_j^i & (a11)_j^i \end{bmatrix}, \{d_m\}_j = \begin{Bmatrix} ((u_N)_m)_j \\ ((v_N)_m)_j \\ (v_c)_j \end{Bmatrix}, \tag{13a}$$

for the Neumann problems, $(DM_{mn})^i_j, \{d_m\}_j$ is modified as

$$(DM_{mn})^i_j = \begin{bmatrix} (s1_{mn})^i_j & (s2_{mn})^i_j & ((b21)_m)^i_j \\ (t1_{mn})^i_j & (t2_{mn})^i_j & ((b31)_m)^i_j \\ ((b12)_n)^i_j & ((b13)_n)^i_j & (b11)^i_j \end{bmatrix}, \{d_m\}_j = \begin{Bmatrix} ((\sigma_N)_m)_j \\ ((\tau_N)_m)_j \\ (\sigma_c)_j \end{Bmatrix}, \tag{13b}$$

these coefficients $(a11)^i_j, ((a12)_n)^i_j, ((a13)_n)^i_j, (b11)^i_j, ((b12)_n)^i_j, ((b13)_n)^i_j$ are defined in Appendix B. Additionally, $((a21)_m)^i_j = (u1^c_m)^i_j, ((a31)_m)^i_j = (v1^c_m)^i_j, ((b21)_m)^i_j = (s1^c_m)^i_j, ((b31)_m)^i_j = (t1^c_m)^i_j$, and $(u1^c_m)^i_j, (v1^c_m)^i_j, (s1^c_m)^i_j, (t1^c_m)^i_j$ are also defined in Appendix B, but λ_n should be replaced by λ_c. By adding corner degree of freedom, the unknown coefficients vector is

$$(C_n)^i = \begin{bmatrix} a^i_n & b^i_n & a^i_c \end{bmatrix}^{\mathrm{T}}. \tag{13c}$$

After the corner degree of freedom is included, the previous example was reexamined, the displacement of cornerA, B of the fixed edge was assigned to zero, and 33 harmonics were utilized for analysis, the Tukey window function [15] is selected to smooth the stress oscillation along the fixed edge. The stresses of fixed edge $\bar{A}\bar{B}$ are illustrated in Fig. 11, and the corner stress is significantly increased.

5. Element connection

The function used herein to construct **DM** is the solution that holds only for the upper half-plane. Therefore, the problem with a non-convex domain where the divergent terms induced by exponential increase in some parts of the domain is probably found, and the numerical method may lose accuracy and yield unexpected results. However, a non-convex domain can be divided into several convex sub-domains by introducing certain internal boundaries and the continuity conditions on these internal boundaries can be used to connect the sub-domains. For instance, a simple non-convex domain in Fig. 12, is cut into two convex triangular elements. Since boundaries 1,2,4,5, have the prescribed boundary conditions, for the common boundary line 3, the displacement boundary is selected for an unknown variable. From the equilibrium and compatibility condition, the relationship between the common boundary and other prescribed boundary conditions can easily be established.

From Eqs. (9a)–(9d), concerning the Dirichlet and Neumann problems, the coefficients matrix and prescribed boundary vectors are

$$[DM] \times \{C\} = \{d\}, \tag{14a}$$

$$[FM] \times \{C\} = \{f\}. \tag{14b}$$

By eliminating the unknown term $\{C\}$ of Eqs. (14a) and (14b), the relation between the boundary value $\{d\}$ and $\{f\}$ is expressed as:

$$[KM] \times \{d\} = \{f\}, \tag{15}$$

where $[KM] = [FM] \times [DM]^{-1}$.

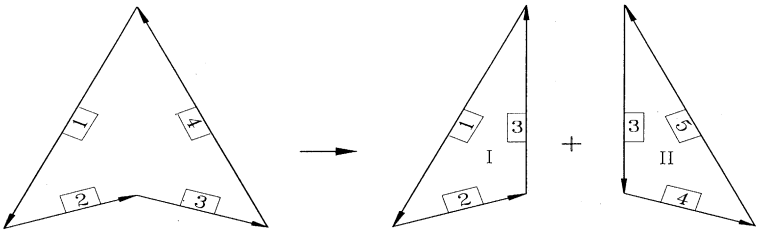

Fig. 12. A non-convex domain divided into two convex sub-domains.

Instead of using matrix form, the relationship of $\{d\},\{f\}$ of elements I and II, is written as:

$$\begin{bmatrix} K_{11} & K_{12} & K_{13} \\ K_{21} & K_{22} & K_{23} \\ K_{31} & K_{32} & K_{33} \end{bmatrix}^{\mathrm{I}} \begin{Bmatrix} d_1 \\ d_2 \\ d_3 \end{Bmatrix}^{\mathrm{I}} = \begin{Bmatrix} f_1 \\ f_2 \\ f_3 \end{Bmatrix}^{\mathrm{I}}, \tag{16a}$$

$$\begin{bmatrix} K_{33} & K_{34} & K_{35} \\ K_{43} & K_{44} & K_{45} \\ K_{53} & K_{54} & K_{55} \end{bmatrix}^{\mathrm{II}} \begin{Bmatrix} d_3 \\ d_4 \\ d_5 \end{Bmatrix}^{\mathrm{II}} = \begin{Bmatrix} f_3 \\ f_4 \\ f_5 \end{Bmatrix}.^{\mathrm{II}} \tag{16b}$$

The equilibrium equations of the common boundary line 3 of elements I and II are

$$[K_{31}]^{\mathrm{I}}\{d_1\}^{\mathrm{I}} + [K_{32}]^{\mathrm{I}}\{d_2\}^{\mathrm{I}} + [K_{33}]^{\mathrm{I}}\{d_3\}^{\mathrm{I}} = \{f_3\}^{\mathrm{I}}, \tag{17a}$$

$$[K_{33}]^{\mathrm{II}}\{d_3\}^{\mathrm{II}} + [K_{34}]^{\mathrm{II}}\{d_4\}^{\mathrm{II}} + [K_{35}]^{\mathrm{II}}\{d_5\}^{\mathrm{II}} = \{f_3\},^{\mathrm{II}} \tag{17b}$$

where

$$\{d_3\}^{\mathrm{I}} = \begin{Bmatrix} (u_N)_3 \\ (v_N)_3 \end{Bmatrix}^{\mathrm{I}}, \{f_3\}^{\mathrm{I}} = \begin{Bmatrix} (\sigma_N)_3 \\ (\tau_N)_3 \end{Bmatrix}^{\mathrm{I}}, \{d_3\}^{\mathrm{II}} = \begin{Bmatrix} (u_N)_3 \\ (v_N)_3 \end{Bmatrix}^{\mathrm{II}}, \{f_3\}^{\mathrm{II}} = \begin{Bmatrix} (\sigma_N)_3 \\ (\tau_N)_3 \end{Bmatrix}^{\mathrm{II}}. \tag{18}$$

The vector of Fourier harmonics in the proposed approach, such as $\{d\},\{f\}$, defined on any boundary are directional. For example, Fig. 12, illustrates that the direction of the common boundary line 3 in element I is in the opposite direction of element II. The continuity conditions in which all the Fourier harmonics must be transformed are define in the same direction. For the cosine expansion, the transformation can be completed by simply changing the sign of the even harmonics of the vector. Herein, a transformation on any vector $\{A\}$ is defined as

$$\left\{\bar{A}_m\right\} = \left\{(-1)^{m+1} \times A_m\right\}, \tag{19}$$

on the common boundary of element II, while the transformed vectors $\{u_N\}^{\mathrm{II}},\{v_N\}^{\mathrm{II}},\{\sigma_N\}^{\mathrm{II}},\{\tau_N\}^{\mathrm{II}}$ are all defined in the positive direction of line 3. The continuity conditions can be written as:

$$\left\{(u_N)_3\right\}^{\mathrm{I}} + \left\{(\bar{u}_N)_3\right\}^{\mathrm{II}} = 0, \tag{20a}$$

$$\left\{(v_N)_3\right\}^{\mathrm{I}} + \left\{(\bar{v}_N)_3\right\}^{\mathrm{II}} = 0, \tag{20b}$$

$$\left\{(\sigma_N)_3\right\}^{\mathrm{I}} = \left\{(\bar{\sigma}_N)_3\right\}^{\mathrm{II}}, \tag{20c}$$

$$\left\{(\tau_N)_3\right\}^{\mathrm{I}} = \left\{(\bar{\tau}_N)_3\right\}^{\mathrm{II}}. \tag{20d}$$

For displacement boundary and force boundary, defined as Eq. (18), the continuity conditions can be written more concisely as:

$$\{d_3\}^{\mathrm{I}} + \left\{\bar{d}_3\right\}^{\mathrm{II}} = 0, \tag{21a}$$

$$\{f_3\}^{\mathrm{I}} = \left\{\bar{f}_3\right\}^{\mathrm{II}}, \tag{21b}$$

from Eqs. (16a), (16b) and Eqs. (20a)–(20d), the common boundary displacement can be expressed as:

$$[\aleph]\{d_3\} = \{\Re\}, \tag{22}$$

where

$$[\aleph] = [K_{33}]^{\mathrm{I}} + \left[\tilde{\bar{K}}_{33}\right], \tag{23a}$$

$$[\Re] = -\left([K_{31}]^{\mathrm{I}}\{d_1\}^{\mathrm{I}} + [K_{32}]^{\mathrm{I}}\{d_2\}^{\mathrm{I}}\right) + \left(\left[\bar{K}_{34}\right]^{\mathrm{II}}\{d_4\}^{\mathrm{II}} + \left[\bar{K}_{35}\right]^{\mathrm{II}}\{d_5\}^{\mathrm{II}}\right), \tag{23b}$$

$\bar{K}, \tilde{K}$ represent the "row transformation" and "column transformation" of K as

$$\bar{K} = \left[\frac{(-1)^m K_{mn}}{(-1)^{m+1} K_{mn}}\right], \tag{24a}$$

$$\tilde{K} = \left[(-1)^n K_{mn} \middle| (-1)^{n+1} K_{mn}\right]. \tag{24b}$$

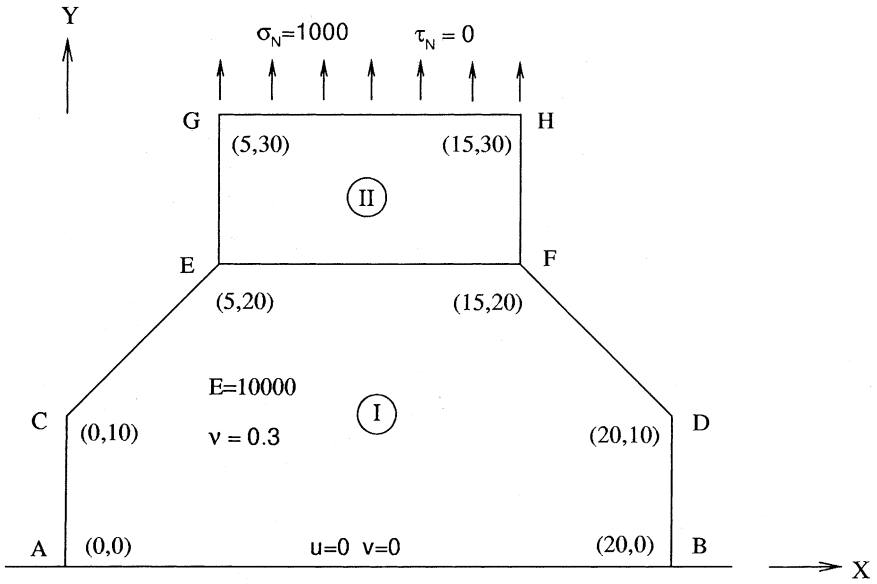

Fig. 13. Connection of non-convex domain under axial load.

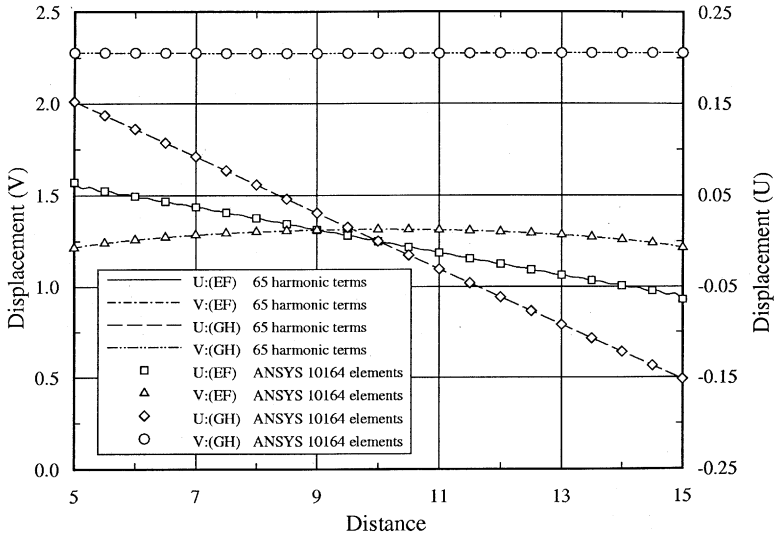

Fig. 14. Comparing of displacements along line *EF*, *GH*.

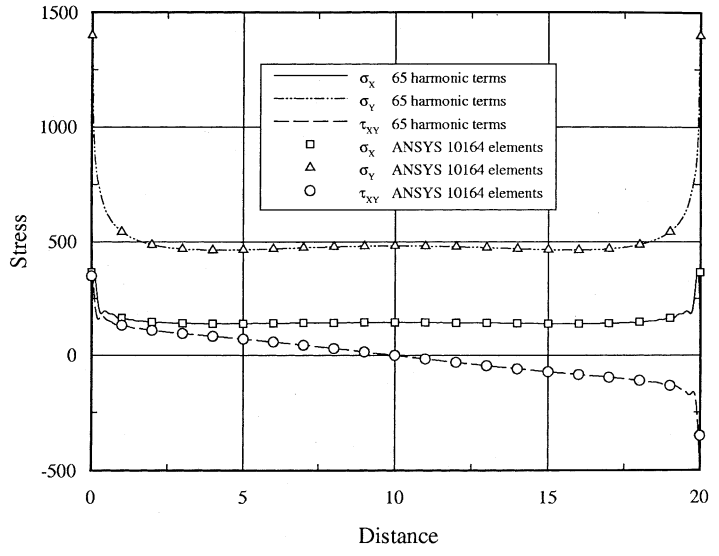

Fig. 15. Comparison of stress along fix edge *AB*.

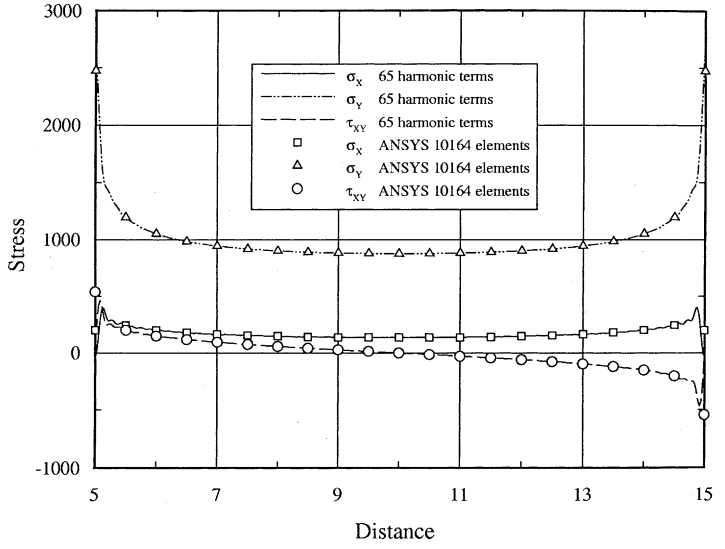

Fig. 16. Comparison of stress along connection edge *EF*.

The example of the non-convex domain, divide into two sub-domains, with uniform distributed load and fixed edge (Fig. 13). The 65 harmonics was used to analyze the problem, and results were compared to ANSYS with 10164 high-order elements. The results from two methods were compared with the displacement along the top edge and common boundary in Fig. 14. Nearly the same results are obtained in both the two methods. The stresses along the fixed edge calculated by the proposed method matches the ANSYS solution but exhibit little oscillation near the corner (Fig. 15). Finally, comparing the stresses in the interior of the domain, the proposed method reaches almost the same solution from the ANSYS results (Fig. 16).

6. Conclusions

This work presents a simple and straightforward method, using the Fourier series, applying the plane elasticity boundary value problem with arbitrary boundary conditions for the polygonal domain. The

solution function of the governing equation with constant coefficients is analytically derived. Meanwhile, the efficient Fast Fourier Transform is used to calculate the discretely prescribed boundary conditions. These conditions give the proposed method highly efficient. Additionally, less degrees of freedom are required than most available numerical methods. Finally, the method proposed herein has the following merits:

1. Little memory and computational effort is necessary, since no numerical integration is involved and less degrees of freedom is required.
2. Only one element is required for a convex domain, while a non-convex domain can be partitioned into several convex sub-domains. This fact suggests that the proposed method provide meshless input that can save considerable effort in problem modeling.
3. Since boundaries are approximated, errors arise only along boundaries. In the interior of the domain, the solution at each point is highly accurate.
4. The Gibb's phenomenon induced by the discrepant boundary conditions results in stress oscillation on the fixed edge. However, the regularization technique can be improved the problem.
5. After incorporating the corner singularity, the stress convergence rate of corner is significantly enhanced.

The current approach has demonstrated the efficiency and accuracy in the presented paper. By the incorporation of the plate-bending problem, the proposed approach analyze the plated structure is feasible.

Appendix A. The calculation of $C_{mn}^{p_n}$, $D_{mn}^{p_n}$, $C_{mn}^{q_n}$, $D_{mn}^{q_n}$

The coefficients of Eqs. (5a)–(5d) can be calculated by the following integration:

$$\text{For } m \neq 1, \quad C_{mn}^{p_n} = \frac{2}{l_i}\int_0^{l_i} \mathrm{e}^{-p_n y}\cos(\lambda_n x)\cos(\alpha_m s)\,\mathrm{d}s,$$

$$D_{mn}^{p_n} = \frac{2}{l_i}\int_0^{l_i} \mathrm{e}^{-p_n y}\sin(\lambda_n x)\cos(\alpha_m s)\,\mathrm{d}s.$$

The fact that, we always calculate the responses on line i due to the input on line j, accounts for why we can omit the superscripts i, j without losing the clarity. With respect to Fig. 2, the coordinate of any point (x, y) on line i can be written as

$$x = x_0 + s\cos\gamma_{ij},$$
$$y = y_0 + s\sin\gamma_{ij},$$

where (x_0, y_0) denotes the coordinate of the starting point of the line i, s represents the distance measured from (x_0, y_0) along i, and γ_{ij} is the angle between the lines$j$ and i. Hence, we have

$$C_{mn}^{p_n} = \mathrm{e}^{-p_n y_0}\left[\cos(\lambda_n x)(ccm + ccp) - \sin(\lambda_n x)(ssm + ssp)\right],$$
$$D_{mn}^{p_n} = \mathrm{e}^{-p_n y_0}\left[\sin(\lambda_n x)(ccm + ccp) + \cos(\lambda_n x)(ssm + ssp)\right],$$

and ccm, ccp, ssm, ssp represent as

$$ccm = \frac{1}{l_i}\frac{1}{(p_n s)^2 + \theta_m^2}\left\{\theta_m \mathrm{e}^{-p_n \sin\gamma_{ij} l_i}\sin(\theta_m l_i) + p_n s\left[1 - \mathrm{e}^{-p_n \sin\gamma_{ij} l_i}\cos(\theta_m l_i)\right]\right\},$$
$$ccp = \frac{1}{l_i}\frac{1}{(p_n s)^2 + \theta_p^2}\left\{\theta_p \mathrm{e}^{-p_n \sin\gamma_{ij} l_i}\sin(\theta_p l_i) + p_n s\left[1 - \mathrm{e}^{-p_n \sin\gamma_{ij} l_i}\cos(\theta_p l_i)\right]\right\},$$
$$ssm = \frac{1}{l_i}\frac{1}{(p_n s)^2 + \theta_m^2}\left\{\theta_m \times \left[1 - \mathrm{e}^{-p_n \sin\gamma_{ij} l_i}\cos(\theta_m l_i)\right] - p_n s \mathrm{e}^{-p_n \sin\gamma_{ij} l_i}\sin(\theta_m l_i)\right\}$$
$$ssp = \frac{1}{l_i}\frac{1}{(p_n s)^2 + \theta_p^2}\left\{\theta_p\left[1 - \mathrm{e}^{-p_n \sin\gamma_{ij} l_i}\cos(\theta_p l_i)\right] - p_n s \mathrm{e}^{-p_n \sin\gamma_{ij} l_i}\sin(\theta_p l_i)\right\},$$

where $p_n s = p_n \sin\gamma_{ij}, \theta_m = \lambda_n \cos\gamma_{ij} - \alpha_m, \theta_p = \lambda_n \cos\gamma_{ij} + \alpha_m$

$$\text{for} \quad m = 1, \quad C_{mn}^{p_n} = \frac{2}{l_i}\int_0^{l_i} \mathrm{e}^{-p_n y}\cos(\lambda_n x)\,\mathrm{d}s,$$
$$D_{mn}^{p_n} = \frac{2}{l_i}\int_0^{l_i} \mathrm{e}^{-p_n y}\sin(\lambda_n x)\,\mathrm{d}s.$$

For a constant term, it more easily integrates into $C_{mn}^{p_n}, D_{mn}^{p_n}$ as

$$n = 0, \quad C_{mn}^{p_n} = \frac{1}{l_i}\int_0^{l_i} \mathrm{e}^{-p_0 x}\cos(\alpha_m s)\,\mathrm{d}s,$$
$$D_{mn}^{p_n} = \frac{1}{l_i}\int_0^{l_i} \mathrm{e}^{-q_0 y}\cos(\alpha_m s)\,\mathrm{d}s,$$

to calculate $C_{mn}^{q_n}, D_{mn}^{q_n}$, it only needs to replaces p_n with q_n in ccm, ccp, ssm, ssp.

Appendix B. The calculation of (a11), (a12), (a13), (b11), (b12), (b13)

From Eqs. (3a), (3b), (4a)–(4d), (5a)–(5d), the values i, j are omitted according to the reason has mentioned earlier. Therefore, all of the coefficients can be illustrated as

$$u1_{mn} = D_{mn}^{p_n} \times \cos\gamma_{ij} + c_n \times C_{mn}^{p_n} \times \sin\gamma_{ij},$$
$$u2_{mn} = D_{mn}^{q_n} \times \cos\gamma_{ij} + d_n \times C_{mn}^{q_n} \times \sin\gamma_{ij},$$
$$v1_{mn} = D_{mn}^{p_n} \times \sin\gamma_{ij} - c_n \times C_{mn}^{p_n} \times \cos\gamma_{ij},$$
$$v2_{mn} = D_{mn}^{q_n} \times \sin\gamma_{ij} - d_n \times C_{mn}^{q_n} \times \cos\gamma_{ij},$$
$$s1_{mn} = \frac{Et}{1-v^2} \times \left\{ \left[\lambda_n(\sin^2\gamma_{ij} + v \times \cos^2\gamma_{ij}) - p_n c_n(\cos^2\gamma_{ij} + v \times \sin^2\gamma_{ij})\right] C_{mn}^{p_n} + (1-v) \times (p_n + c_n\lambda_n) D_{mn}^{p_n} \sin\gamma_{ij}\cos\gamma_{ij} \right\},$$
$$s2_{mn} = \frac{Et}{1-v^2} \times \left\{ \left[\lambda_n(\sin^2\gamma_{ij} + v \times \cos^2\gamma_{ij}) - q_n d_n(\cos^2\gamma_{ij} + v \times \sin^2\gamma_{ij})\right] C_{mn}^{q_n} + (1-v) \times (q_n + d_n\lambda_n) D_{mn}^{q_n} \times \sin\gamma_{ij}\cos\gamma_{ij} \right\},$$
$$t1_{mn} = \frac{Et}{2(1+v)}\left[-(p_n + c_n\lambda_n)(\sin^2\gamma_{ij} - \cos^2\gamma_{ij}) D_{mn}^{p_n} + (\lambda_n + c_n p_n) C_{mn}^{p_n} \sin 2\gamma_{ij} \right],$$
$$t2_{mn} = \frac{Et}{2(1+v)}\left[-(q_n + d_n\lambda_n)(\sin^2\gamma_{ij} - \cos^2\gamma_{ij}) D_{mn}^{q_n} + (\lambda_n + d_n q_n) C_{mn}^{q_n} \sin 2\gamma_{ij} \right].$$

For the corner function, it yields

$$(a11) = \left[\mathrm{e}^{-p_c y_j^i}\sin(\lambda_c x_j^i)\right]\sin\gamma_{ij} - \left[c_c \mathrm{e}^{-p_c y_j^i}\cos(\lambda_c x_j^i)\right]\cos\gamma_{ij},$$
$$(a12)_n = \left[\mathrm{e}^{-p_n y_j^i}\sin(\lambda_n x_j^i)\right]\sin\gamma_{ij} - \left[c_n \mathrm{e}^{-p_n y_j^i}\cos(\lambda_n x_j^i)\right]\cos\gamma_{ij},$$
$$(a13)_n = \left[\mathrm{e}^{-q_n y_j^i}\sin(\lambda_n x_j^i)\right]\sin\gamma_{ij} - \left[d_n \mathrm{e}^{-q_n y_j^i}\cos(\lambda_n x_j^i)\right]\cos\gamma_{ij},$$
$$(b11) = \frac{Et}{1-v^2}\left\{ \left[\lambda_c(\sin^2\gamma_{ij} + v \times \cos^2\gamma_{ij}) - c_c p_c(\cos^2\gamma_{ij} + v \times \sin^2\gamma_{ij})\right] C_c^{p_c} + (1-v)(p_c + c_c\lambda_c)\sin\gamma_{ij}\cos\gamma_{ij} D_c^{p_c} \right\},$$
$$(b12)_n = \frac{Et}{1-v^2}\left\{ \left[\lambda_n(\sin^2\gamma_{ij} + v \times \cos^2\gamma_{ij}) - c_n p_n(\cos^2\gamma_{ij} + v \times \sin^2\gamma_{ij})\right] C_n^{p_n} + (1-\bar{v})(p_n + c_n\lambda_n)\sin\gamma_{ij}\cos\gamma_{ij} D_n^{p_n} \right\},$$

$$(b13)_n = \frac{Et}{1-v^2}\left\{\left[\lambda_n(\sin^2\gamma_{ij} + v\times\cos^2\gamma_{ij}) - d_n q_n(\cos^2\gamma_{ij} + v\times\sin^2\gamma_{ij})\right]C_n^{q_n} + (1-v)(q_n + d_n\lambda_n)\sin\gamma_{ij}\cos\gamma_{ij}D_n^{q_n}\right\},$$

where

$$C_c^{p_c} = e^{-p_c y_j^i}\cos(\lambda_c x_j^i) \quad D_c^{p_c} = e^{-p_c y_j^i}\sin(\lambda_c x_j^i),$$
$$C_n^{p_n} = e^{-p_n y_j^i}\cos(\lambda_c x_j^i) \quad D_n^{p_n} = e^{-p_n y_j^i}\sin(\lambda_c x_j^i),$$
$$C_n^{q_n} = e^{-q_n y_j^i}\cos(\lambda_c x_j^i) \quad D_n^{q_n} = e^{-q_n y_j^i}\sin(\lambda_c x_j^i),$$

where t is the thickness of plate.

References

[1] M.D. Bird, C.R. Steele, Separated solution procedure for bending of circular plate with circular holes, ASME. Appl. Mech. Rev. 44 (1991) 27–35.
[2] M.D. Bird, C.R. Steele, A solution procedure for Laplace's equation on multiply connected circular domains, ASME J. Appl. Mech. 59 (1992) 398–404.
[3] F.M.W. Kwok, L.C. Kang, C.R. Steele, Mode III fracture mechanics analysis with Fourier series method, ASME. Appl. Mech. Rev. 44 (1991) 166–170.
[4] F.M.W. Kwok, Fourier Series Method for Cracks in Polygonal and Shells of Revolution, Ph.D. Thesis, Dissertation, Department of Mechanical Engineering, Stanford University, 1994.
[5] L.C. Kang, A Fourier series method for polygonal domains; large element computation for plates, Ph.D. Thesis, Dissertation, Department of Mechanical Engineering, Stanford University, 1992.
[6] C.H. Wu, A Fourier series method for stability of shallow shells with one large element computations for plates, Ph.D. Thesis, Dissertation, Department of Mechanical Engineering, Stanford University, 1993.
[7] L.C. Kang, C.H. Wu, C.R. Steele, Fourier series for polygonal plate bending; a very large plate element, Appl. Math. Comput. 67 (1995) 157–225.
[8] Y.C. Fu, C.R. Steele, Fourier series solution for the Dugdale crack in a cylindrical shell, ASME J. Appl. Mech. 62 (1995) 533–535.
[9] Y.C. Fu, A large element computation for polygonal-shaped plates, shallow shells and cylindrical shells with the Fourier series and state-variable method, Ph.D. Thesis, Dissertation, Department of Mechanical Engineering, Stanford University, 1996.
[10] D.J. Gorman, Vibration Analysis of Plates by the Superposition Method, World Scientific, Singapore, 1999.
[11] G.H. Hardy, Divergent Series, Oxford University Press, London, 1949.
[12] C. Lanczos, Appl. Analysis, Prentice-Hall, Englewood Cliffs, NJ, 1956.
[13] S.P. Timoshenko, J.N. Goodier, Theory of Elasticity, McGraw-Hill, New York, 1951.
[14] ANSYS version 5.1, User's Manual, Swanson analysis systems, Inc. Houston, PA, 1994.
[15] D.G. Childers, A.E. Durling, Digital Filtering and Signal Processing, West Publishing Company, New York, 1975.